SRDiff: Single Image Super-Resolution with Diffusion Probabilistic Models

Haoying Li[1] , **Yifan Yang**[1] , **Meng Chang**[1] , **Huajun Feng**[1*] , **Zhihai Xu**[1] , **Qi Li**[1] and **Yueting Chen**[1]

[1]Zhejiang University

{lhaoying,yangyifan,changm,fenghj,xuzhi,liqi,chenyt}@zju.edu.cn

Abstract

Single image super-resolution (SISR) aims to reconstruct high-resolution (HR) images from the given low-resolution (LR) ones, which is an ill-posed problem because one LR image corresponds to multiple HR images. Recently, learning-based SISR methods have greatly outperformed traditional ones, while suffering from over-smoothing, mode collapse or large model footprint issues for PSNR-oriented, GAN-driven and flow-based methods respectively. To solve these problems, we propose a novel single image super-resolution diffusion probabilistic model (SRDiff), which is the first diffusion-based model for SISR. SRDiff is optimized with a variant of the variational bound on the data likelihood and can provide diverse and realistic SR predictions by gradually transforming the Gaussian noise into a super-resolution (SR) image conditioned on an LR input through a Markov chain. In addition, we introduce residual prediction to the whole framework to speed up convergence. Our extensive experiments on facial and general benchmarks (CelebA and DIV2K datasets) show that 1) SRDiff can generate diverse SR results in rich details with state-of-the-art performance, given only one LR input; 2) SRDiff is easy to train with a small footprint; and 3) SRDiff can perform flexible image manipulation including latent space interpolation and content fusion.

1 Introduction

Over the years, single image super-resolution (SISR) has drawn active attention due to its wide applications in computer vision such as object recognition [Fookes *et al.*, 2012; Sajjadi *et al.*, 2017], remote sensing [Li *et al.*, 2009], surveillance monitoring [Fang *et al.*, 2019; Park *et al.*, 2020] and so on. SISR aims to recover high-resolution (HR) images from low-resolution (LR) ones, which is an ill-posed problem, for multiple HR images can be degenerated to one LR image as shown in Figure 1.
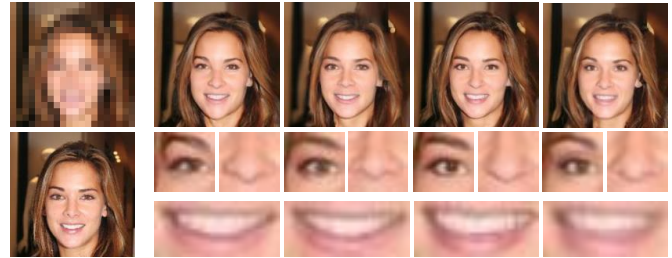
---

*Corresponding Author

Figure 1: Random SR (8x) predictions generated by our method. LR/HR image is shown on top top/bottom left. The right columns are diverse SR predictions and their facial regions, which are different from each other in expressions and attributes. For example, the first nose looks flat, while the third looks straight.

To establish the mapping between HR and LR images, lots of deep learning-based methods emerge and could be categorized into three main types: PSNR-oriented, GAN-driven and flow-based methods. PSNR-oriented methods [Dong *et al.*, 2015; Lim *et al.*, 2017; Zhang *et al.*, 2018b; Qiu *et al.*, 2019; Guo *et al.*, 2020] are trained with simple distribution assumption-based losses (e.g., Laplacian for L_1 and Gaussian for L_2) and achieve excellent PSNR. However, these losses tend to drive the SR result to an average of several possible SR predictions, causing **over-smoothing** images with high-frequency information loss. One groundbreaking solution to tackle the over-smoothing problem is GAN-driven methods [Cheon *et al.*, 2018; Kim *et al.*, 2019; Ledig *et al.*, 2017; Wang *et al.*, 2018], which combine content losses (e.g., L_1 and L_2) and adversarial losses to obtain sharper SR images with better perceptual quality. However, GAN-driven methods are easy to fall into **mode collapse**, which leads to a single generated SR sample without diversity. Additionally, GAN-based training process is not easy to converge and requires an extra discriminator which is not used in inference. Flow-based methods [Lugmayr *et al.*, 2020] directly account for the ill-posed problem with an invertible encoder, which maps HR images to the flow-space latents conditioned on LR inputs. Trained with a negative log-likelihood loss, flow-based methods avoid training instability but suffer from **extremely large footprint and high train-**

ing cost due to the strong architectural constraints to keep the bijection between latents and data.

Lately, the successful adoptions of diffusion probabilistic models (diffusion models for short) in image synthesis [Ho *et al.*, 2020] and speech synthesis [Kong *et al.*, 2020; Chen *et al.*, 2021] witness the power of diffusion models in generative tasks. The diffusion models use a Markov chain to convert data x_0 to latent variable x_T in simple distribution (e.g., Gaussian) by gradually adding noise ϵ in the diffusion process, and predict the noise ϵ in each diffusion step to recover the data x_0 through a learned reverse process. Diffusion models are trained by optimizing a variant of the variational lower bound, which is efficient and avoids the mode collapse encountered by GAN.

In this paper, we propose a novel single image super-resolution diffusion probabilistic model (SRDiff) to tackle the over-smoothing, mode collapse and huge footprint problems in previous SISR models. Specifically, 1) to extract the image information in LR image, SRDiff exploits a pretrained low-resolution encoder to convert LR image into hidden condition. 2) To generate the HR image conditioned on LR image, SRDiff employs a conditional noise predictor to recover x_0 iteratively. 3) To speed up convergence and stabilize training, SRDiff introduces residual prediction by taking the difference between the HR and LR image as the input x_0 in the first diffusion step, making SRDiff focus on restoring high-frequency details. To the best of our knowledge, SRDiff is the first diffusion-based SR model and has several advantages:

- **Diverse and high-quality outputs**: SRDiff converts Gaussian white noise into an SR prediction through a Markov chain, which does not suffer from mode collapse and can generate diverse and high-quality SR results.

- **Stable and efficient training with small footprint**: Although the data distribution of HR image is hard to estimate, SRDiff admits a variant of the variational bound maximization and applies residual prediction. Compared with GAN-driven methods, SRDiff is stably trained with a single loss and does not need any extra module (e.g., discriminator, which is only used in training). Compared with flow-based methods, SRDiff has no architectural constraints and thus enjoys benefits from small footprint and fast training.

- **Flexible image manipulation**: SRDiff can perform flexible image manipulation including latent space interpolation and content fusion using both diffusion process and reverse process, which shows broad application prospects.

Our extensive experiments on CelebA [Liu *et al.*, 2015a] and DIV2K [Timofte *et al.*, 2018] datasets show that 1) SRDiff can reconstruct multiple SR results given one LR input and outperform state-of-the-art SISR methods; 2) SRDiff only has 1/4 parameters and is stable and fast to train (about 30 hours on 1 GPU until convergence) compared with SRFlow; 3) we can manipulate the generated SR images in latent space to obtain more diverse outputs.

2 Related Works

2.1 Single Image Super-Resolution

Recently, deep learning methods have become widely adopted to single image super-resolution (SISR) and we categorize them into three types: PSNR-oriented and GAN-driven and flow-based methods. The training goal of **PSNR-oriented methods** is to minimize the mean squared error (MSE) between the ground truth and the SR image recovered from the LR image. SRCNN [Dong *et al.*, 2015] sets a precedent of end-to-end mapping between the LR and HR images. Kim *et al.* [2016b; 2016a] then apply residual neural network techniques to SR tasks and deepen the network. Some works[Lim *et al.*, 2017; Zhang *et al.*, 2018b; Qiu *et al.*, 2019; Guo *et al.*, 2020] enhance the SR performance by carefully adjusting network structures and losses. **GAN-driven methods** [Cheon *et al.*, 2018; Kim *et al.*, 2019] solve the over-smoothing problem towards perceptual restrictions [Rad *et al.*, 2019; Zhang *et al.*, 2019]. The pioneer work is SRGAN [Ledig *et al.*, 2017], using SRResNet [Ledig *et al.*, 2017] and perceptual loss as well as the adversarial loss to improve the naturalness of the recovered image. ESRGAN [Wang *et al.*, 2018] further enhances it with network adjustments of structure and loss function. The first **flow-based methods** is SR-Flow [Lugmayr *et al.*, 2020], which builds an invertible neural network to transform a Gaussian distribution into an HR image space instead of modeling one single output and inherently resolves the pathology of the original "one-to-many" SR problem.

2.2 Diffusion models

Diffusion probabilistic models [Sohl-Dickstein *et al.*, 2015; Ho *et al.*, 2020] are a kind of generative models using a Markov chain to transform latent variables in simple distributions (e.g., Gaussian) to data in complex distributions. Researchers find it useful to tackle "one-to-many" problems and synthesize high-quality results in speech synthesis tasks [Kong *et al.*, 2020] and image synthesis fields [Ho *et al.*, 2020]. However, to the best of our knowledge, diffusion models have not yet been used in image reconstruction fields like super-resolution. In this paper, we propose our impressive work, SRDiff, building on diffusion models to generate diverse SR images with a single LR input, and solving over-smoothing, mode collapse and large footprint issues together.

3 Diffusion Model

In this section, to provide a basic understanding of diffusion probabilistic models (diffusion model for short) [Ho *et al.*, 2020], we first briefly review its formulation.

A diffusion model is a kind of generative model which adopts parameterized Markov chain trained using variational inference to gradually generate data x_0 in complex distribution from a latent variable x_T in simple distribution, where T is the total diffusion step. We set $x_t \in \mathbb{R}^d$ to be the results of each diffusion timestep $t \in \{1, 2, ..., T\}$ and x_t shares the same dimension d as that of x_0. As shown in Figure 2, a diffusion model is composed of two processes: the **diffusion process** and the **reverse process**.
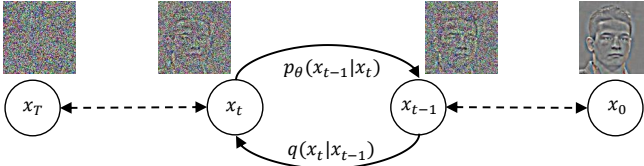
Figure 2: Overview of two processes in SRDiff. The diffusion process is from right to left and the reverse process is from left to right. θ in p_θ denotes the learnable components including conditional noise predictor and low-resolution encoder in SRDiff.

The posterior $q(x_1, \cdots, x_T | x_0)$, named as the **diffusion process**, converts the data distribution $q(x_0)$ to the latent variable distribution $q(x_T)$, and is fixed to a Markov chain which gradually adds Gaussian noise ϵ to the data according to a variance schedule $\beta_1, \cdots, \beta_T$:

$$q(x_1, \cdots, x_T | x_0) := \prod_{t=1}^{T} q(x_t | x_{t-1}),$$

$$q(x_t | x_{t-1}) := \mathcal{N}(x_t; \sqrt{1-\beta_t} x_{t-1}, \beta_t \mathbf{I}),$$

where β_t is a small positive constant and could be regarded as constant hyperparameters. Setting $\alpha_t := 1 - \beta_t$, $\bar{\alpha}_t := \prod_{s=1}^{t} \alpha_s$, the diffusion process allows sampling x_t at an arbitrary timestep t in closed form:

$$q(x_t | x_0) = \mathcal{N}(x_t; \sqrt{\bar{\alpha}_t} x_0, (1-\bar{\alpha}_t)\mathbf{I}), \tag{1}$$

which can be further reparameterized as

$$x_t(x_0, \epsilon) = \sqrt{\bar{\alpha}_t} x_0 + \sqrt{1-\bar{\alpha}_t}\epsilon, \ \epsilon \sim \mathcal{N}(\mathbf{0}, \mathbf{I}). \tag{2}$$

The **reverse process** transforms the latent variable distribution $p_\theta(x_T)$ to the data distribution $p_\theta(x_0)$ parameterized by θ. It is defined by a Markov chain with learned Gaussian transitions beginning with $p(x_T) = \mathcal{N}(x_T; \mathbf{0}, \mathbf{I})$:

$$p_\theta(x_0, \cdots, x_{T-1} | x_T) := \prod_{t=1}^{T} p_\theta(x_{t-1} | x_t),$$

$$p_\theta(x_{t-1} | x_t) := \mathcal{N}(x_{t-1}; \mu_\theta(x_t, t), \sigma_\theta(x_t, t)^2 \mathbf{I}), \tag{3}$$

In training phase, we maximize the variational lower bound (ELBO) on negative log likelihood and introduce KL divergence and variance reduction [Ho *et al.*, 2020]:

$$\mathbb{E}[-\log p_\theta(x_0)] \le L := \mathbb{E}_q \Big[\underbrace{D_{KL}(q(x_T|x_0) \,\|\, p(x_T))}_{L_T}$$

$$+ \sum_{t>1} \underbrace{D_{KL}(q(x_{t-1}|x_t, x_0) \,\|\, p_\theta(x_{t-1}|x_t))}_{L_{t-1}} \underbrace{- \log p_\theta(x_0|x_1)}_{L_0} \Big]. \tag{4}$$

This transformation requires a direct comparison between $p_\theta(x_{t-1}|x_t)$ and its corresponding diffusion process posteriors. Setting $\tilde{\mu}_t(x_t, x_0) := \frac{\sqrt{\bar{\alpha}_{t-1}}\beta_t}{1-\bar{\alpha}_t} x_0 + \frac{\sqrt{\alpha_t}(1-\bar{\alpha}_{t-1})}{1-\bar{\alpha}_t} x_t$, we have

$$q(x_{t-1}|x_t, x_0) = \mathcal{N}(x_{t-1}; \tilde{\mu}_t(x_t, x_0), \tilde{\beta}_t \mathbf{I}). \tag{5}$$

Eq. (1), (3) and (5) assure that all KL divergences in Eq. (4) are comparisons between Gaussians. With $\sigma_\theta^2 = \tilde{\beta}_t = \frac{1-\bar{\alpha}_{t-1}}{1-\bar{\alpha}_t}\beta_t$ for $t > 1$, $\tilde{\beta}_1 = \beta_1$, and constant C, we have

$$L_{t-1} = \mathbb{E}_q \left[\frac{1}{2\sigma_t^2} \|\tilde{\mu}_t(x_t, x_0) - \mu_\theta(x_t, t)\|^2 \right] + C.$$

For simplicity, the training procedure minimizes the variant of the ELBO with x_0 and t as inputs:

$$\min_\theta L_{t-1}(\theta) = \mathbb{E}_{x_0, \epsilon, t} \big[\|\epsilon - \epsilon_\theta(\sqrt{\bar{\alpha}_t} x_0 + \sqrt{1-\bar{\alpha}_t}\epsilon, \ t)\|^2 \big], \tag{6}$$

where ϵ_θ is a noise predictor.

In inference, we first sample an $x_T \sim \mathcal{N}(x_T; \mathbf{0}, \mathbf{I})$, and then sample $x_{t-1} \sim p_\theta(x_{t-1}|x_t)$ according to Eq. (3), where

$$\mu_\theta(x_t, t) := \frac{1}{\sqrt{\alpha_t}} \left(x_t - \frac{\beta_t}{\sqrt{1-\bar{\alpha}_t}}\epsilon_\theta(x_t, t) \right),$$

$$\sigma_\theta(x_t, t) := \tilde{\beta}_t^{\frac{1}{2}}, t \in \{T, T-1, ..., 1\}. \tag{7}$$

4 SRDiff

As depicted in Figure 2, SRDiff is built on a T-step diffusion model which contains two processes: diffusion process and reverse process. Instead of predicting the HR image directly, we apply residual prediction to predict the difference between the HR image x_H and the upsampled LR image $up(x_L)$ and denote the difference as input residual image x_0. Diffusion process converts the x_0 into a latent x_T in Gaussian distribution by gradually adding Gaussian noise ϵ as implied in Eq. (2). According to Eq. (3) and (7), the reverse process is determined by ϵ_θ, which is a conditional noise predictor with an RRDB-based [Wang *et al.*, 2018] low-resolution encoder (LR encoder for short) $\mathcal{D}$, as shown in Figure 3. The reverse process converts a latent variable x_T to a residual image x_r by iteratively denoising in finite step T using the conditional noise predictor ϵ_θ, conditioned on the hidden states encoded from LR image by the LR encoder $\mathcal{D}$. The SR image is reconstructed by adding the generated residual image x_r to the upsampled LR image $up(x_L)$. Therefore, the goal of ϵ_θ is to predict the noise ϵ added at each diffusion timestep in the diffusion process[1].

In the following subsections, we will introduce architectures of the conditional noise predictor, LR encoder, training and inference.

Conditional Noise Predictor The conditional noise predictor ϵ_θ predicts noise added in each timestep of the diffusion process conditioned on the LR image information, according to Eq. (6) and (7). As shown in Figure 3, we use U-Net as the main body, taking 3-channel x_t, the diffusion timestep $t \in \{1, 2, ..., T-1, T\}$ and the output of LR encoder as inputs. First, x_t is transformed to hidden through a 2D-convolution block which consists of one 2D-convolutional layer and Mish activation [Misra, 2019]. Then the LR information is fused with the 2D-convolution block output hidden. Following Ho *et al.* [2020], we transform the timestep

---
[1]Instead of the original L_2 in Eq. (6), we use L_1 for better training stability following Chen *et al.* [2021].
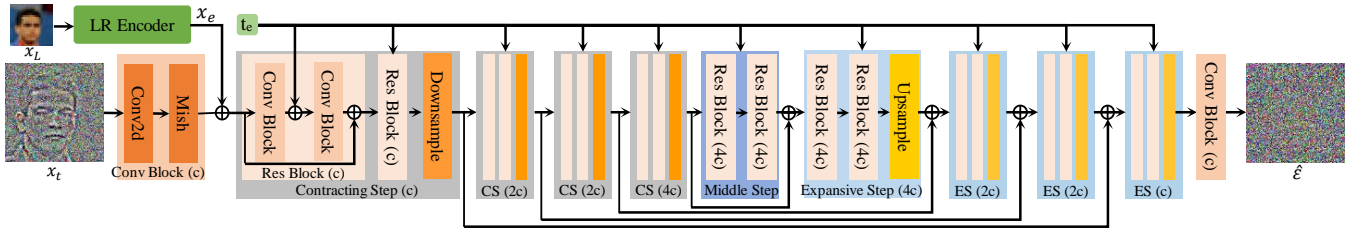
Figure 3: The architecture of conditional noise predictor in SRDiff. The content in parentheses (c, 2c and 4c) after the block name means the channel size of each block. "Conv Block", "Res Block", "Downsample" and "Upsample" denote 2D-Convolution block, residual block, downsampling layer and upsampling layer respectively; "CS" and "ES" denote "Contracting Step" and "Expansive Step" respectively.

Algorithm 1 Training

1: **Input**: LR image and its corresponding HR image pairs $P = \{(x_L^k, x_H^k)\}_{k=1}^K$, total diffusion step T
2: **Initialize**: randomly initialized conditional noise predictor ϵ_θ and pretrained LR encoder $\mathcal{D}$
3: **repeat**
4:      Sample $(x_L,\ x_H) \sim P$
5:      Upsample x_L as $up(x_L)$, compute $x_r = x_H - up(x_L)$
6:      Encode LR image x_L as $x_e = \mathcal{D}(x_L)$
7:      Sample $\epsilon \sim \mathcal{N}(\mathbf{0}, \mathbf{I})$, and $t \sim \text{Uniform}(\{1, \cdots, T\})$
8:      Take gradient step on
        $\nabla_\theta \|\epsilon - \epsilon_\theta(x_t, x_e, t)\|, x_t = \sqrt{\bar{\alpha}_t}x_r + \sqrt{1 - \bar{\alpha}_t}\epsilon$
9: **until** converged

Algorithm 2 Inference

1: **Input**: LR image x_L, total diffusion step T
2: **Load**: conditional noise predictor ϵ_θ and LR encoder $\mathcal{D}$
3: Sample $x_T \sim \mathcal{N}(\mathbf{0}, \mathbf{I})$
4: Upsample x_L to $up(x_L)$
5: Encode LR image x_L as $x_e = \mathcal{D}(x_L)$
6: **for** $t = T, T-1, \cdots, 1$ **do**
7:      Sample $z \sim \mathcal{N}(\mathbf{0}, \mathbf{I})$ if $t > 1$, else $z = 0$
8:      Compute x_{t-1} using Eq. (7):
        $x_{t-1} = \frac{1}{\sqrt{\alpha_t}}\left(x_t - \frac{1-\alpha_t}{\sqrt{1-\bar{\alpha}_t}}\epsilon_\theta(x_t, x_e, t)\right) + \sigma_\theta(x_t, t)z$
9: **end for**
10: **return** $x_0 + up(x_L)$ as SR prediction

---

t to the timestep embedding t_e using the Transformer sinusoidal positional encoding [Vaswani *et al.*, 2017]. Then the last output hidden and t_e are fed into the contracting path, one middle step and the expansive path successively. The contracting path and expansive path both consist of four steps, each of which successively applies two residual blocks and one downsampling/upsampling layer. To reduce the model size, we only double the channel size in the second and the fourth contracting steps and halve the spatial sizes of the feature map in each contracting step. The downsampling layer in contracting path is a two-stride 2D convolution and the upsampling layer in expansive path is 2D transposed convolution. The middle step consists of two residual blocks, which is inserted between the contracting and expansive paths. Besides, the inputs of each expansive step concatenate the corresponding feature map from the contracting path. Finally, a 2D-convolution block is applied to generate $\hat{\epsilon}$ in timestep $t-1$ as the predicted noise, which is then used to recover x_{t-1} according to Eq. (3) and (7). Our conditional noise predictor is easy and stable to train due to the multi-scale skip connection. Moreover, it combines local and global information through the contracting and expansive path.

LR Encoder An LR encoder encodes the LR information x_e, which is added to each reverse step to guide the generation to the corresponding HR space. In this paper, we choose the RRDB architecture following SRFlow [Lugmayr *et al.*, 2020], which employs the residual-in-residual structure and multiple dense skip connections without batch normalization layers. In particular, we abandon the last convolution layer of the RRDB architecture because we do not aim at the concrete

SR results but the hidden LR image information.

Training In the training phase, as illustrated in Algorithm 1, the input LR-HR image pairs in the training set are used to train SRDiff with the total diffusion step T (Line 1). We randomly initialize the conditional noise predictor ϵ_θ and the RRDB based LR encoder $\mathcal{D}$ is pretrained by L_1 loss function (Line 2). We then sample a mini-batch of LR-HR image pairs from the training set (Line 4) and compute the residual image x_r (Line 5). The LR images are encoded by the LR encoder as x_e (Line 6), which is fed into the noise predictor ϵ_θ together with t and x_T. Then we sample ϵ from the standard Gaussian distribution and t from the integer set $\{1, \cdots, T\}$ (Line 7). We optimize the noise predictor by taking gradient step on Eq. (6) (Line 8).

Inference A T-step SRDiff inference takes an LR image x_L as input (Line 1), as illustrated in Algorithm 2. We sample a latent variable x_T from the standard Gaussian distribution (Line 3) and upsample x_L with bicubic kernel (Line 4). Different from the training procedure, we encode the LR image x_L to x_e by the LR encoder only once before the iteration begins (Line 5) and apply it in every iteration, which speeds up the inference. The iterations start from $t = T$ (Line 6), and each iteration outputs a residual image with a different noise level, which gradually declines as t decreases. For $t > 1$, we sample z from standard Gaussian distribution (Line 7) and compute x_{t-1} using the noise predictor ϵ_θ with x_t, x_e and t as inputs (Line 8). Then for $t = 1$, we set $z = 0$ (Line 6) and x_0 is the final residual prediction (Line 10). An SR image is recovered by adding the residual image x_0 on the upsampled LR image $up(x_L)$.
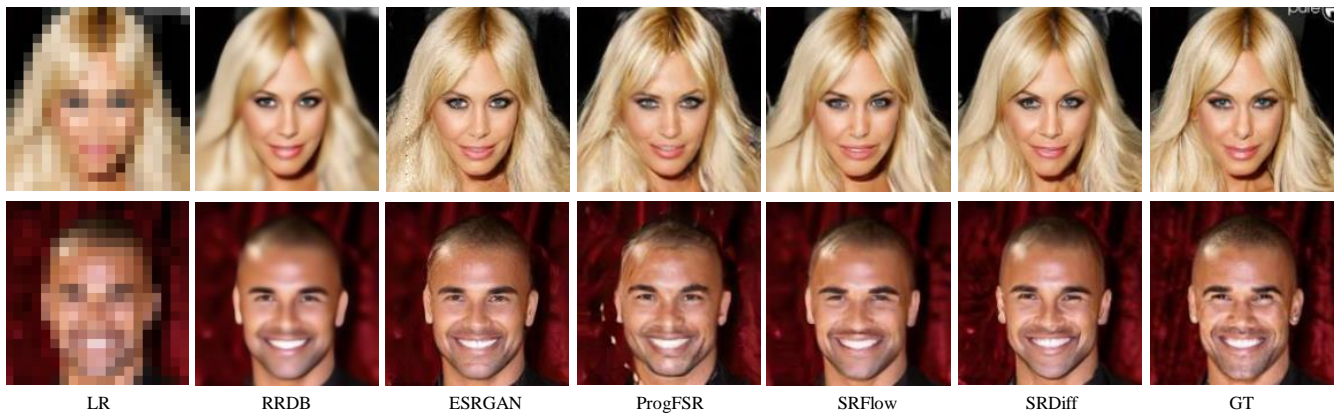
Figure 4: Face SR $8\times$ visual results. SRDiff generates rich details than RRDB and SRFlow, avoids artifacts (e.g., grids on the woman's hair and stripes on man's head) encountered by ESRGAN and ProgFSR and maintain consistency with the ground truth.
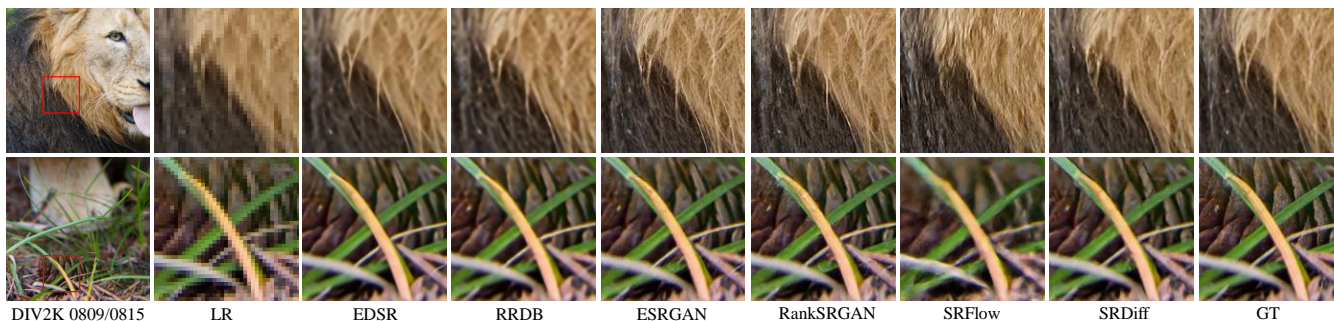

Figure 5: General SR ($4\times$) visual results. SRDiff produces more natural textures, e.g., animal fur, and grass texture, and also less unpleasant artifacts, e.g., speckles on the yellow grass by ESRGAN and RankSRGAN. Only SRDiff maintains the brown streak on the yellow grass, which is consistent with the ground truth.

5 Experiments

In this section, we first describe the experimental settings including datasets, model configurations and details in training and inference. Then we report experimental results and conduct some analyses.

5.1 Experimental Settings

Datasets SRDiff is trained and evaluated on face SR ($8\times$) and general SR ($4\times$) tasks. For face SR, we use Celeb-Faces Attributes Dataset (CelebA) [Liu *et al.*, 2015b], which is a large-scale face attributes dataset with more than 200K celebrity images. The images in this dataset cover large pose variations and background clutter. In this paper, we use the whole training set which consists of 162,770 images for training and evaluate on 5000 images from the test split following SRFlow [Lugmayr *et al.*, 2020]. We central-crop the aligned patches[2] and resize them to 160×160 as HR ground truth using standard MATLAB bicubic kernel. To obtain the corresponding LR images, we downsample the HR images with bicubic kernel. For ProgFSR [Kim *et al.*, 2019], we use pro-

---

[2]https://drive.google.com/drive/folders/
0B7EVK8r0v71pWEZsZE9oNnFzTm8

gressive bilinear kernel introduced in its original paper for a fair comparison.

For General SR, we use the DIV2K [Timofte *et al.*, 2018] and Flickr2K [Timofte *et al.*, 2018]. These datasets consist of high-resolution RGB images with a large diversity of contents. In training, we use the whole training data (800 images) in DIV2K and whole images in Flickr2K (2650 images). Then we crop each image into patches with a size of 160×160 as HR ground truth following SRFlow. To obtain the corresponding LR images, we downsample the HR images with bicubic kernel. For evaluation, we use the whole validation data (100 images) in DIV2K. We downsample the HR images with bicubic kernel to obtain the LR images and directly apply SISR methods on the LR images to obtain the SR predictions without cropping.

Model Configuration Our SRDiff model consists of a 4-step conditional noise predictor and an LR encoder with multiple RRDB blocks. The number of channels c in the first contracting step is set to 64. The numbers of RRDB blocks in the LR encoder are set to 8 and 15 for CelebA and DIV2K respectively and the channel size is set to 32. For diffusion process and reverse process, we set the diffusion step T to 100 and our noise schedule $\beta_1, ..., \beta_T$ follows Nichol *et al.* [2021], which

is proved to be beneficial for training. We also explore the model performance under different T and c in Section 5.3.

Training and Evaluation Firstly, we pretrain the LR encoder $\mathcal{D}$ using an L_1 loss for 100k iterations for the sake of efficiency. The training of the conditional noise predictor uses Eq. (6) as loss term and Adam [Kingma and Ba, 2014] as optimizer, with batch size 16 and learning rate 2×10^{-4}, which is halved every 100k steps. The entire SRDiff takes about 34/45 hours (300k/400k steps) to train on 1 GeForce RTX 2080Ti with 11GB memory for CelebA/DIV2K respectively.

Beside the well-known evaluation metrics PSNR and SSIM [Wang *et al.*, 2004], we also evaluate our SRDiff on LPIPS [Zhang *et al.*, 2018a], LR-PSNR [Lugmayr *et al.*, 2020] and the pixel standard deviation σ. LPIPS is recently introduced as a reference-based image quality evaluation metric, which computes the perceptual similarity between the ground truth and the SR images. LR-PSNR is computed as the PSNR between the downsampled SR image and the LR one indicating the consistency with the LR image. The pixel standard deviation σ indicates diversity in the SR output.

5.2 Performance

In this subsection, we evaluate SRDiff by comparing with several state-of-the-art SR methods on face SR ($8\times$) and general SR ($4\times$) tasks. The detailed configurations of baseline models can be found in their original papers.

	Methods	↑PSNR	↑SSIM	↓LPIPS	↑LR-PSNR	↑ σ
Bicubic	Bicubic	23.38	0.65	0.484	34.66	0.00
	RRDB	26.89	0.78	0.220	48.01	0.00
	ESRGAN	23.24	0.66	0.115	39.91	0.00
	SRFlow	25.32	0.72	0.108	50.73	5.21
	SRDiff	25.38	0.74	0.106	52.34	6.13
Prog.	ProgFSR	24.21	0.69	0.126	42.19	0.00
	SRFlow	25.28	0.72	0.109	51.15	5.32
	SRDiff	25.32	0.73	0.106	51.41	6.19

Table 1: Results for 8× SR of faces on CelebA. The first column indicates how LR images degenerate from HR ones and *Prog.* means the progressive linear kernel from ProgFSR.

Face SR We compare SRDiff with RRDB [Wang *et al.*, 2018], ESRGAN [Wang *et al.*, 2018], ProgFSR [Kim *et al.*, 2019] and SRFlow ($\tau = 0.8$) [Lugmayr *et al.*, 2020][3]. RRDB is trained by only L_1 loss and can be regarded as a PSNR-oriented method. The evaluation results are shown in Table 1, which reveals that SRDiff outperforms previous works in term of most of the evaluation metrics, and can generate high-quality and diverse SR images with strong LR-consistency. Specifically, 1) as shown in Figure 4, compared with PSNR-oriented methods, SRDiff reconstructs clearer textures, and

---

[3]Due to inconsistent patch size, we retrain all these baseline models from scratch on our pre-processed CelebA dataset with released codes. SRFlow uses the same patch size as our model, but we cannot obtain the same patch with its released image example, and therefore, we also have to re-train it.

compared with GAN-driven methods, SRDiff avoids artifacts and the results look more natural; and 2) as shown in Figure 1, SRDiff provides diverse and realistic SR predictions given only one LR input. Every SR prediction is a complete portrait of a human face with rich details and maintains consistency with the input LR image. Moreover, SRDiff uses fewer model parameters (12M) than SRFlow (40M) and only takes about 30 hours until converge as described in Section 5.1, while SRFlow needs 5 days, which demonstrates that SRDiff is training-efficient and can achieve comparable performance with a small model footprint since SRDiff does not impose any architectural constraints to guarantee bijection. Compared with GAN-driven methods, SRDiff does not need any extra module (e.g., discriminator) in training.

Methods	↑PSNR	↑SSIM	↓LPIPS	↑LR-PSNR	↑ σ
Bicubic	26.70	0.77	0.409	38.70	0.00
EDSR	28.98	0.83	0.270	54.89	0.00
RRDB	29.44	0.84	0.253	49.20	0.00
RankSRGAN	26.55	0.75	0.128	42.33	0.00
ESRGAN	26.22	0.75	0.124	39.03	0.00
SRFlow	27.09	0.76	0.120	49.96	5.14
SRDiff	27.41	0.79	0.136	55.21	6.09

Table 2: Results for 4× SR of general images on DIV2K.

General SR We also evaluate SRDiff on general SR ($4\times$) compared with EDSR [Lim *et al.*, 2017], RRDB, ESRGAN, RankSRGAN [Zhang *et al.*, 2019] and SRFlow ($\tau = 0.9$) with their official released pretrained models[4]. As shown in Table 2, SRDiff achieves better quantitative results than the previous methods for most evaluation metrics (PSNR, SSIM and LR-PSNR) and comparable LPIPS, which reveals the effectiveness and great potential of our method. Figure 5 shows that SRDiff balances sharpness and naturalness well and produces strong consistency with the LR image. In contrast, PSNR-oriented methods (EDSR and RRDB) and SR-Flow, smear the edges of the objects, and GAN-driven methods (ESRGAN and RankSRGAN) introduce more artifacts.

T	c	*Res.*	↑PSNR	↑SSIM	↓LPIPS	↑LR-PSNR	↓*Steps*
100	64	√	25.38	0.74	0.106	52.34	300k
25	64	√	25.12	0.71	0.109	52.17	300k
200	64	√	25.41	0.74	0.106	52.31	300k
1000	64	√	25.43	0.75	0.105	52.35	300k
100	32	√	25.15	0.72	0.108	52.20	300k
100	128	√	25.40	0.74	0.106	52.37	300k
100	64	×	24.88	0.70	0.111	51.90	600k

Table 3: Ablations of SRDiff for faces SR ($8\times$) on CelebA. T, c and *Res.* denote the total diffusion step, channel size of the noise predictor, and the residual prediction respectively.

---

[4]Except RRDB which is trained from scratch with L_1 loss as that in Face SR.

Source	Target	Input
t = 30	t = 50	t = 70

(a) SRDiff applying on content fusion task.

$\lambda = 0.0$	$\lambda = 0.4$	$\lambda = 0.8$	$\lambda = 1.0$

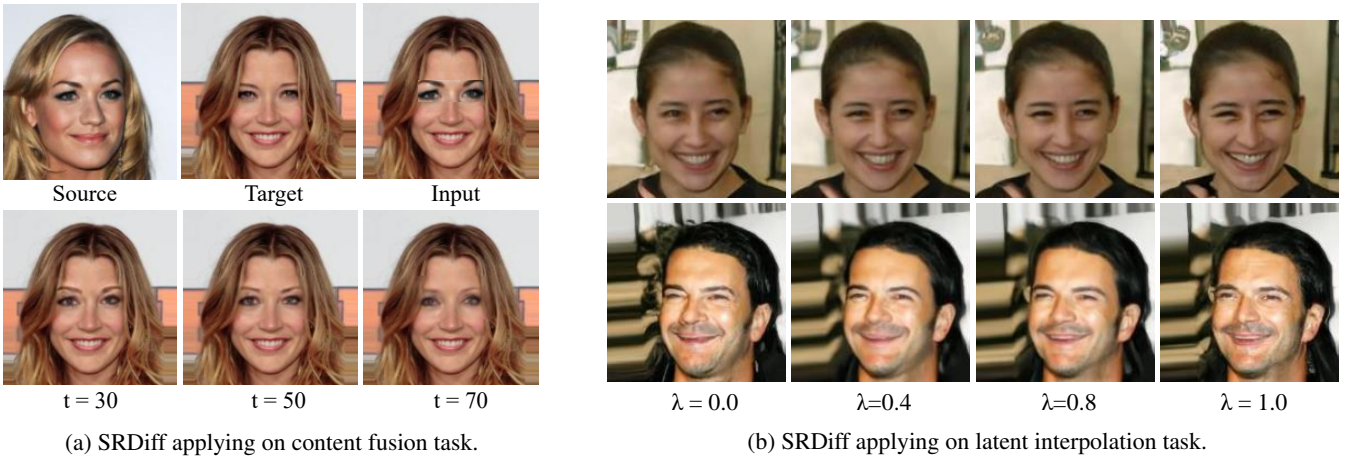(b) SRDiff applying on latent interpolation task.

Figure 6: Extended applications of SRDiff.

5.3 Ablation Study

To probe the influences of the total diffusion step T, noise predictor channel size c and the effectiveness of residual prediction, we conduct some ablation studies as illustrated in Table 3. From row 1, 2, 3 and 4, we can see that the image quality is enhanced as total diffusion steps increases. From row 1, 5 and 6, we can see that larger model width results in better performance. However, larger total diffusion steps and model width both lead to slower inference, and therefore, we choose $T = 100$ and $c = 64$ as the default setting after trading off. Row 1 and 7 indicate that the residual prediction not only greatly enhances the image quality but also speeds up the training, which demonstrates the effectiveness of residual prediction.

5.4 Extensions

In this subsection, we explore some extended applications including content fusion and latent space interpolation.

Content Fusion SRDiff is applicable in content fusion tasks, which aim to generate an image by fusing contents from two source images, e.g., an eye-source image and a face-source image providing the eye and face contents respectively. In this paragraph, we use SRDiff to conduct face content fusion by a demonstration of fusing one's eyes with another one's face. The procedure of content fusion is shown in Algorithm 3. First, we directly fuse a face image x_f by replacing the eye region of the face-source image x_{face} with that of the eye-source image x_{eye} and compute the differences between x_f and the upsampled LR face-source image $up(x_L)$ to get the residual x_r. Second, x_r goes through a $\bar{t}$-step diffusion process, which outputs the $x_{\bar{t}}$ in latent space. Then $x_{\bar{t}}$ is denoised to an HR residual using the conditional noise predictor iterated from $\bar{t}$ to 0 with the LR face-source information encoded by the LR encoder, which ensures the compatibility of the two contents. Then we get the fused SR image by adding the SR residual to $up(x_L)$. Finally, we replace the eye region of the face-source image with that of the SR face image and preserve the non-manipulated face. As shown in Figure 6a, we set different timesteps $t \in \{30, 50, 70\}$ and

find that the eye region of the fusion result is more similar to the eye-source image when t is small, and is closer to the face-source image as t becomes larger.

Algorithm 3 Content Fusion

1: **Input**: eye-source image x_{eye}, face-source image x_{face}, diffusion step $\bar{t}$.
2: **Load**: conditional noise predictor ϵ_θ and LR encoder $\mathcal{D}$.
3: Replace the eye region of x_{face} by the that of x_{eye} to form the initial fused image x_f
4: Upsample the LR face-source image x_L as $up(x_L)$
5: Compute $x_r = x_f - up(x_L)$
6: Put x_r into the diffusion process and compute $x_{\bar{t}}(x_r, \epsilon) = \sqrt{\bar{\alpha}_{\bar{t}}}x_r + \sqrt{1 - \bar{\alpha}_{\bar{t}}}\epsilon$, $\epsilon \sim \mathcal{N}(\mathbf{0}, \mathbf{I})$
7: Encode x_L as $x_e = \mathcal{D}(x_L)$
8: **for** $t = \bar{t}, \cdots, 1$ **do**
9:     Sample $z \sim \mathcal{N}(\mathbf{0}, \mathbf{I})$ if $t > 1$, else $z = 0$
10:     Compute $x_{t-1} = \frac{1}{\sqrt{\alpha_t}}\left(x_t - \frac{1-\alpha_t}{\sqrt{1-\bar{\alpha}_t}}\epsilon_\theta(x_t, x_e, t)\right) + \sigma_\theta(x_t, t)z$
11: **end for**
12: Compute the SR face prediction $x_H = x_0 + up(x_L)$
13: Crop the eye region of x_H and insert it to the corresponding eye region of x_{face} to generate x_{fused}
14: **return** x_{fused} as the content fusion result

Latent Space Interpolation Given an LR image, SRDiff can manipulate its prediction by latent space interpolation, which linearly interpolates the latents of two SR predictions and generate a new one. Let $x_{\bar{t}}, x'_{\bar{t}} \sim q(x_{\bar{t}}|x_0)$ and we decode the latent $\bar{x}_{\bar{t}} = \lambda x_{\bar{t}} + (1 - \lambda)x'_{\bar{t}}$ by the reverse process, which feeds $\bar{x}_{\bar{t}}$ into the noise predictor with the LR information encoded by LR encoder iteratively. Then, we add the output residual result to the $up(x_L)$ to obtain the interpolated SR prediction. We set $\bar{t} = 50$ and $\lambda \in \{0.0, 0.4, 0.8, 1.0\}$. It could be observed in Figure 6b that with λ approaching to 1.0, the woman's expression becomes closer to x_t, which is the top right image holding a big laugh. In the same way, the man's mouth turns wider and bigger from $\lambda = 0.0$ to $\lambda = 1.0$. The trend of the interpolated images shows the effectiveness of SRDiff in latent space interpolation. The detailed algo-

rithm of latent space interpolation is shown in Algorithm 4.

Algorithm 4 Latent Space Interpolation

1: **Input**: LR image x_L, diffusion step $\bar{t}$, $\lambda \in [0, 1]$
2: **Load**: conditional noise predictor ϵ_θ and LR encoder $\mathcal{D}$
3: Sample $x_{\bar{t}}, x'_{\bar{t}} \sim \mathcal{N}(\mathbf{0}, \mathbf{I})$
4: Compute $\bar{x}_t = \lambda x_{\bar{t}} + (1 - \lambda)x'_{\bar{t}}$
5: Upsample x_L as $up(x_L)$
6: Encode x_L as $x_e = \mathcal{D}(x_L)$
7: **for** $t = \bar{t}, \cdots, 1$ **do**
8:     Sample $z \sim \mathcal{N}(\mathbf{0}, \mathbf{I})$ if $t > 1$, else $z = 0$
9:     Compute $x_{t-1} = \frac{1}{\sqrt{\alpha_t}}\left(x_t - \frac{1-\alpha_t}{\sqrt{1-\bar{\alpha}_t}}\epsilon_\theta(\bar{x}_t, x_e, t)\right) + \sigma_\theta(x_t, t)z$
10: **end for**
11: **return** the interpolated SR face prediction $x_H = x_0 + up(x_L)$ as the latent interpolation results

---

6 Conclusion

In this paper, we proposed SRDiff, which is the first diffusion-based model for single image super-resolution to the best of our knowledge. Our work exploits a Markov chain to convert HR images to latents in simple distribution and then generate SR predictions in the reverse process which iteratively denoises the latents using a noise predictor conditioned on LR information encoded by the LR encoder. To speed up convergence and stabilize training, SRDiff introduces residual prediction. Our extensive experiments on both face and general datasets demonstrate that SRDiff can generate diverse and realistic SR images and avoids over-smoothing and mode collapse issues that occurred in PSNR-oriented methods and GAN-driven methods respectively. Moreover, SRDiff is stable to train with small footprint and without an extra discriminator. Besides, SRDiff allows for flexible image manipulation including latent space interpolation and content fusion.

In the future, we will further improve the performance of the diffusion-based SISR model and speed up the inference. We will also extend our work to more image restoration tasks (e.g., image denoising, deblurring and dehazing) to verify the potential of diffusion models in the image restoration domain.

References

[Chen *et al.*, 2021] Nanxin Chen, Yu Zhang, Heiga Zen, Ron J Weiss, Mohammad Norouzi, and William Chan. Wavegrad: Estimating gradients for waveform generation. In *ICLR*, 2021.

[Cheon *et al.*, 2018] Manri Cheon, Jun-Hyuk Kim, Jun-Ho Choi, and Jong-Seok Lee. Generative adversarial network-based image super-resolution using perceptual content losses. In *Proceedings of ECCV*, pages 0–0, 2018.

[Dong *et al.*, 2015] Chao Dong, Chen Change Loy, Kaiming He, and Xiaoou Tang. Image super-resolution using deep convolutional networks. *IEEE transactions on pattern analysis and machine intelligence*, 38(2):295–307, 2015.

[Fang *et al.*, 2019] Hongbao Fang, Shankun Yao, Qixin Chen, Chunyan Liu, Yuqi Cai, Shanshan Geng, Yang Bai, Zhiqi Tian, Amanda L Zacharias, Takanori Takebe, et al. De novo-designed near-infrared nanoaggregates for super-resolution monitoring of lysosomes in cells, in whole organoids, and in vivo. *ACS nano*, 13(12):14426–14436, 2019.

[Fookes *et al.*, 2012] Clinton Fookes, Frank Lin, Vinod Chandran, and Sridha Sridharan. Evaluation of image resolution and super-resolution on face recognition performance. *Journal of Visual Communication and Image Representation*, 23(1):75–93, 2012.

[Guo *et al.*, 2020] Yong Guo, Jian Chen, Jingdong Wang, Qi Chen, Jiezhang Cao, Zeshuai Deng, Yanwu Xu, and Mingkui Tan. Closed-loop matters: Dual regression networks for single image super-resolution. In *CVPRW*, pages 5407–5416, 2020.

[Ho *et al.*, 2020] Jonathan Ho, Ajay Jain, and Pieter Abbeel. Denoising diffusion probabilistic models. *NeurIPS*, 2020.

[Kim *et al.*, 2016a] Jiwon Kim, Jung Kwon Lee, and Kyoung Mu Lee. Accurate image super-resolution using very deep convolutional networks. In *CVPR*, 2016.

[Kim *et al.*, 2016b] Jiwon Kim, Jung Kwon Lee, and Kyoung Mu Lee. Deeply-recursive convolutional network for image super-resolution. In *CVPR*, pages 1637–1645, 2016.

[Kim *et al.*, 2019] Deokyun Kim, Minseon Kim, Gihyun Kwon, and Dae-Shik Kim. Progressive face super-resolution via attention to facial landmark. *arXiv preprint arXiv:1908.08239*, 2019.

[Kingma and Ba, 2014] Diederik P Kingma and Jimmy Ba. Adam: A method for stochastic optimization. *arXiv preprint arXiv:1412.6980*, 2014.

[Kong *et al.*, 2020] Zhifeng Kong, Wei Ping, Jiaji Huang, Kexin Zhao, and Bryan Catanzaro. Diffwave: A versatile diffusion model for audio synthesis. *arXiv preprint arXiv:2009.09761*, 2020.

[Ledig *et al.*, 2017] Christian Ledig, Lucas Theis, Ferenc Huszár, Jose Caballero, Andrew Cunningham, Alejandro Acosta, Andrew P Aitken, Alykhan Tejani, Johannes Totz, Zehan Wang, et al. Photo-realistic single image super-resolution using a generative adversarial network. *CVPR*, 2017.

[Li *et al.*, 2009] Feng Li, Xiuping Jia, Donald Fraser, and Andrew Lambert. Super resolution for remote sensing images based on a universal hidden markov tree model. *IEEE Transactions on Geoscience and Remote Sensing*, 48(3):1270–1278, 2009.

[Lim *et al.*, 2017] Bee Lim, Sanghyun Son, Heewon Kim, Seungjun Nah, and Kyoung Mu Lee. Enhanced deep residual networks for single image super-resolution. In *CVPRW*, pages 136–144, 2017.

[Liu *et al.*, 2015a] Ziwei Liu, Ping Luo, Xiaogang Wang, and Xiaoou Tang. Deep learning face attributes in the wild. In *ICCV*, pages 3730–3738, 2015.

[Liu *et al.*, 2015b] Ziwei Liu, Ping Luo, Xiaogang Wang, and Xiaoou Tang. Deep learning face attributes in the wild. In *ICCV*, December 2015.

[Lugmayr *et al.*, 2020] Andreas Lugmayr, Martin Danelljan, Luc Van Gool, and Radu Timofte. Srflow: Learning the super-resolution space with normalizing flow. In *ECCV*, pages 715–732. Springer, 2020.

[Misra, 2019] Diganta Misra. Mish: A self regularized non-monotonic neural activation function. *arXiv preprint arXiv:1908.08681*, 2019.

[Nichol and Dhariwal, 2021] Alexander Quinn Nichol and Prafulla Dhariwal. Improved denoising diffusion probabilistic models, 2021.

[Park *et al.*, 2020] Soohyun Park, Yeongeun Kang, Jeman Park, and Joongheon Kim. Self-controllable super-resolution deep learning framework for surveillance drones in security applications. *EAI Endorsed Transactions on Security and Safety*, 7(23):e5, 2020.

[Qiu *et al.*, 2019] Yajun Qiu, Ruxin Wang, Dapeng Tao, and Jun Cheng. Embedded block residual network: A recursive restoration model for single-image super-resolution. In *ICCV*, pages 4180–4189, 2019.

[Rad *et al.*, 2019] Mohammad Saeed Rad, Behzad Bozorgtabar, Urs-Viktor Marti, Max Basler, Hazim Kemal Ekenel, and Jean-Philippe Thiran. Srobb: Targeted perceptual loss for single image super-resolution. In *ICCV*, pages 2710–2719, 2019.

[Sajjadi *et al.*, 2017] Mehdi SM Sajjadi, Bernhard Scholkopf, and Michael Hirsch. Enhancenet: Single image super-resolution through automated texture synthesis. In *ICCV*, pages 4491–4500, 2017.

[Sohl-Dickstein *et al.*, 2015] Jascha Sohl-Dickstein, Eric A Weiss, Niru Maheswaranathan, and Surya Ganguli. Deep unsupervised learning using nonequilibrium thermodynamics. *arXiv preprint arXiv:1503.03585*, 2015.

[Timofte *et al.*, 2018] Radu Timofte, Shuhang Gu, Jiqing Wu, and Luc Van Gool. Ntire 2018 challenge on single image super-resolution: methods and results. In *CVPR Workshops*, 2018.

[Vaswani *et al.*, 2017] Ashish Vaswani, Noam Shazeer, Niki Parmar, Jakob Uszkoreit, Llion Jones, Aidan N Gomez, Łukasz Kaiser, and Illia Polosukhin. Attention is all you need. In *NeurIPS*, pages 5998–6008, 2017.

[Wang *et al.*, 2004] Zhou Wang, Alan C Bovik, Hamid R Sheikh, and Eero P Simoncelli. Image quality assessment: from error visibility to structural similarity. *IEEE transactions on image processing*, 13(4):600–612, 2004.

[Wang *et al.*, 2018] Xintao Wang, Ke Yu, Shixiang Wu, Jinjin Gu, Yihao Liu, Chao Dong, Chen Change Loy, Yu Qiao, and Xiaoou Tang. Esrgan: Enhanced super-resolution generative adversarial networks. *ECCV*, 2018.

[Zhang *et al.*, 2018a] Richard Zhang, Phillip Isola, Alexei A Efros, Eli Shechtman, and Oliver Wang. The unreasonable effectiveness of deep features as a perceptual metric. *CVPR*, 2018.

[Zhang *et al.*, 2018b] Yulun Zhang, Kunpeng Li, Kai Li, Lichen Wang, Bineng Zhong, and Yun Fu. Image super-resolution using very deep residual channel attention networks. In *ECCV*, pages 286–301, 2018.

[Zhang *et al.*, 2019] Wenlong Zhang, Yihao Liu, Chao Dong, and Yu Qiao. Ranksrgan: Generative adversarial networks with ranker for image super-resolution. In *ICCV*, 2019.